International Journal of Rock Mechanics & Mining Sciences 70 (2014) 59–68

Contents lists available at ScienceDirect

International Journal of Rock Mechanics & Mining Sciences

journal homepage: www.elsevier.com/locate/ijrmms

3D topographic stress perturbations and implications for ground control in underground coal mines

W. Ashley Griffith [a,*], James Becker [b], Krysta Cione [c], Tim Miller [d], Ernian Pan [e]

[a] Department of Earth and Environmental Sciences, University of Texas Arlington, Arlington, TX, USA
[b] Department of Geosciences, University of Akron, Akron, OH, USA
[c] Golder Associates, Pittsburgh, PA, USA
[d] East Fairfield Coal Company, E Lima, OH, USA
[e] Department of Civil Engineering, University of Akron, Akron, OH, USA

ARTICLE INFO

Article history:
Received 29 April 2013
Received in revised form
8 March 2014
Accepted 18 March 2014

Keywords:
Boundary element method
Topography
Ground control
Coal mining
Cutter roof
in situ stress

ABSTRACT

It is well known that the perturbed stress field beneath valleys can result in roof instabilities in shallow underground coal and stone mines. Quantitatively predicting the magnitude of these stress perturbations, particularly beneath complicated three-dimensional (3D) topography, has not become commonplace in mine planning, perhaps due to the complexity and time-consuming nature of the problem. Here we utilize 3D digital elevation models and the 3D boundary element method (BEM) approach to efficiently calculate the pre-mining topographically perturbed stress field in the vicinity of the Carroll Hollow coal mine in eastern Ohio. We find that regions of elevated compressive stress in the mine correspond to areas in which cutter roof failure is a common source of roof instability. Furthermore, both the magnitude and inclination of the principal stresses calculated from the 3D topographic BEM model are found to be consistent with observed failure distributions within the mine. We propose that the approach outlined in this study can be efficiently applied to the mine planning process in order to mitigate or avoid potentially hazardous mining conditions.

1. Introduction

Of the 77 reported fatalities in underground coal mines nationwide from 2007 to 2011, 26 resulted from roof or rib falls [1]. Furthermore, Moebs and Stateham [2] reported that as many as 90% of roof falls in underground mines in the Appalachian Basin occurred in mines beneath stream valleys [2]. While this is a difficult number to confirm, Molinda et al. [3] mapped roof failures in five mines in Pennsylvania and found that 52% of roof failures occurred directly beneath valley bottoms, whereas fewer than 10% of roof falls occurred beneath hills. The same study indicated that valley shape is also an important factor, and risk of roof failure beneath broad valleys is generally greater than beneath sharp v-shaped valleys [3]. The cause of increased roof failure rate beneath valleys has many potential sources, including (1) magnification of the horizontal compressive normal stress and (2) long-term degradation of roof rocks due to fracture and fluid infiltration; however all of these potential sources are directly related to a perturbation in the regional stress field associated with uneven topography. The general relationship between stream valleys and roof instability has been recognized for quite some time [2–5]; however surface topography has not commonly been taken into account quantitatively when planning underground excavations.

Roof stability in underground mines is controlled by the quality and thickness of the rock layers which encase the excavation, the geometry of the excavation, the stress state around the mine excavation, and the presence of pre-existing geologic structures such as joints, faults, and channel sand deposits. Mechanisms of roof instability can be divided into geologic and stress-related mechanisms as well as post-mining degradation of the roof rock due to exposure to fluids. For shallow coal and stone mines, stress-related mechanisms are principally controlled by the greatest horizontal compressive stress, σ_H, in layered sedimentary rocks [6]. Because topography perturbs the stress field in the near surface, particularly where the depth is of the same order of magnitude as the topographic relief, the magnitude and orientation of σ_H, and other stress tensor components, can be extremely heterogeneous throughout the mine; yet no efficient method has been developed to calculate its distribution during the mine planning phase. However, given some basic observations, the state of stress acting on a target layer (coal seam, limestone, etc.) can be

* Correspondence to: Department of Earth and Environmental Sciences, University of Texas Arlington, P.O. Box 19049, Arlington, Texas, 76019, USA.
E-mail address: wagriff@uta.edu (W.A. Griffith).

http://dx.doi.org/10.1016/j.ijrmms.2014.03.013
1365-1609/

predicted with significant confidence *a priori*. Here we study the heterogeneous stress field induced at the scale of an individual mine by modeling the interaction of topography and tectonic stresses using the three-dimensional (3D) boundary element method (BEM) code *Poly3D*. The computed stress fields are evaluated in terms of mapped roof failure mechanisms throughout the mine. The results suggest that the computed stress field accurately represents the state of stress acting on the coal seam before creation of the excavations. Therefore, the approach outlined in this manuscript represents a potentially powerful, efficient means to optimize mine planning in order to minimize potential risks related to stress-related roof failure mechanisms.

2. Previous work

Molinda and Mark [6] listed several factors which commonly result in unplanned roof failures in underground coal mines, including geologic heterogeneities, moisture degradation of the roof rocks, extreme loading conditions, multiple seam mining, and inadequate support. A number of roof fall types, including stack-rock delamination, cutter roof, and spalling roof are typically attributed to large magnitudes of "horizontal stress", the component of normal stress acting parallel to the roof strata [6,7]. Layer–parallel loading leads to buckling of the stratigraphic roof layers. Furthermore, moisture degradation can be enhanced in areas of large horizontal stress due to damage and increased permeability in roof layers, and unstable conditions around geologic defects can likewise be exacerbated by magnified horizontal stress.

The study of the mechanics of failure in undermined strata has been a topic quantitative research for some time. Bucky [8] pioneered the use of a centrifuge to build scale mechanical models of underground openings in stratified rock, and Bucky and Taborelli [9] showed that fractures formed at the mid-span of roof layers are the dominant mechanism of failure under gravitational loading conditions. Evans [10] developed a "Voussoir Beam" model, in which an arched and cracked elastic beam is confined between abutments, to study the failure mechanisms of rock crushing of roof strata at abutments or midspan, buckling of the beam and tensile failure of the beam at midspan, and sliding of the beam at abutments. Many more recent researchers have studied and improved Evans' Voussoir Beam approach in recent years [11–13]; however the model is ultimately two dimensional, and therefore limited in its applicability to complicated mine geometries such as room and pillar mines where stress perturbations associated with adjacent rooms are prone to mechanical interaction. Furthermore, the Voussoir Beam model is difficult to apply successfully where the 3D state of stress is heterogeneous and/or anisotropic.

A significant amount of work across the fields of geology and engineering has shed a great deal of light on the multi-scale nature of the state of stress in the earth's crust. The state of stress in the earth's crust is heterogeneous and anisotropic; yet at the global (crustal) scale, the directions and magnitudes of principal stresses are remarkably systematic, and stress trajectories are largely related to tectonic processes [14–17] (Fig. 1A). For example, in the northeastern United States, the maximum principal horizontal stress (σ_H) follows a NE–SW trend, and in the Appalachian Plateau in eastern Ohio, the location of the current study, σ_H trends approximately N60°E (Fig. 1A). At the regional scale, however, the state of stress may be highly heterogeneous, affected by geologic structures such as faults, and, near the earth's surface, by irregular topography (Fig. 1B). Given that many underground mine workings in the Appalachian Basin region are at depths less than a few hundred meters, stress perturbations at this scale due to topography are of immense importance, as such perturbations may decrease (or increase) the stability of mine workings. Furthermore, once the excavation is introduced in this already heterogeneous stress field, the local stress field is further perturbed (Fig. 1C).

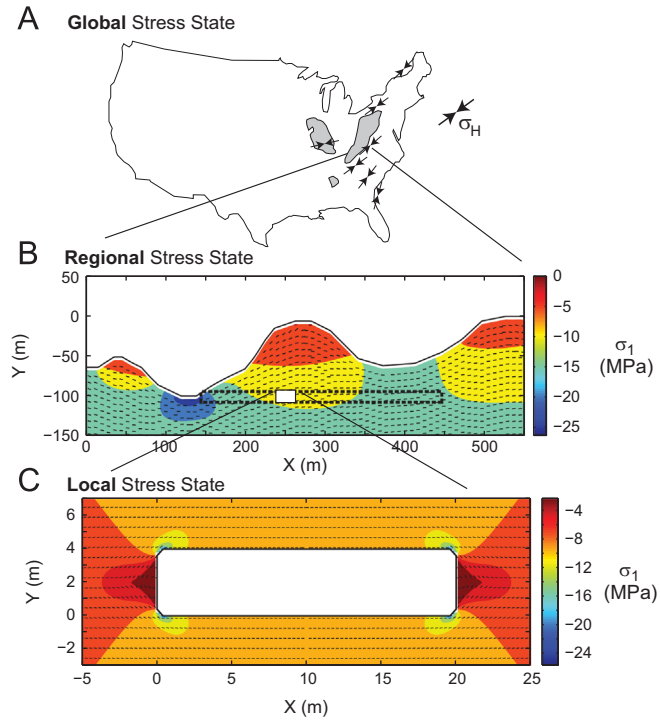

Fig. 1. Nature of the (A) global, (B) regional, and (C) local excavation-scale states of stress. (A) is shown in map view while (B) and (C) are vertical cross-sections.

The importance of topographic effects on subsurface stress has been recognized for some time. Unfortunately, however, perhaps due to the complex nature of the problem, quantitative assessments of the increased risk associated with mining under stream valleys are not customarily made. Empirical estimates of the stress effects of stream valleys [4] have focused on shape factors of the overlying valley, as well as the ratio of excavation depth to total surface relief as critical parameters in the estimation of stability risk; however it is difficult to incorporate the far-field tectonic stress state in such models, as this component of the stress field is independent of local factors such as topography. A number of workers have utilized the method of conformal mapping pioneered by Muskhelishvilli [12] to derive exact closed-form solutions for the elastic stress fields beneath slopes under different loading conditions [18–21]. While such solutions produce quick estimates of subsurface stresses, they are limited to simple idealized topographic shapes. Pan and co-workers [22–25] were able to develop a semi-analytical approach by combining the conformal mapping and the integral equation methods. Under gravitational stress only, they found that beneath irregular, asymmetric valleys and ridges, there can be several locations of local stress maxima and minima which could be potential locations of rock failure [22,24]. They also showed that under a horizontal tectonic stress, the compressive stress on the bottom of the valley could be several times larger (more compressive) than the applied tectonic stress. They further showed that, under combined gravitational and tectonic stresses, a stress concentration could also exist on the shoulder of the ridge [25]. They concluded that the topographically perturbed stress field depended strongly on the depth of the valley, the rock elastic properties, and the orientation of the rock strata [23]. For transversely isotropic rocks for which the plane of anisotropy is horizontal, as is the case for flat-lying sedimentary rocks, the increase of the horizontal compressive stress relative to the background global value can be considerably greater than for the isotropic case. A preliminary application of such findings is on the optimal selection of unlined pressure tunnel alignment [26].

Due to the complex geometry of real topography and room/pillar mines, only a few studies in the mining literature have focused on modeling topographic stress perturbations, using two-dimensional (2D) finite element method (FEM) models [27] or finite difference (FD) codes such as FLAC [28]. Unfortunately complex geometries, particularly in regions in which topography varies significantly in three dimensions, render such FEM and FD methods overly cumbersome to be practically utilized during mine planning. Martel [29] and Martel and Muller [30] extended the BEM method to solve the 2D elastic stresses beneath slopes and long ridges. In their model the state of stress at any point in the subsurface is a result of the superposition of vertical gravitational stress σ_v and the global tectonic stress σ_H. Because the topographic surface is irregular, the gravitational component of stress is non-uniform throughout the model (Fig. 1B). The stress field beneath a topographic surface can be calculated by subtracting the gravitationally induced stresses imposed by the overburden on the underlying material from the stresses in a semi-infinite half plane in which the free surface is coincident with the highest topographic point in the study area (Fig. 1B) [30]). The resulting model is one in which the tractions acting on the topographic free surface are zero, and the stresses beneath the free surface are non-uniform beneath an arbitrary topographic profile. The method of Martel [29] and Martel and Muller [30] has several distinct advantages over previous approaches in that (1) BEM requires discretization of only model boundaries (the topographic surface, underground opening, geologic discontinuities) rather than the entire problem domain, so it is easy to represent any arbitrary topographic surface; (2) it is easy to incorporate tectonic and gravitational stress inputs, if information about the tectonic stress state is known; and (3) the method is easily extendable to 3D using commercially available BEM codes such as *Poly3D* [31]. This latter advantage is particularly critical in regions such as the Appalachian Basin, where surface topography is shaped principally by dendritic drainage patterns which make 2D plane strain models of topography inadequate.

If the mining engineer had *a priori* knowledge of the state of stress as it varies across the entire target layer, he could employ that information to implement any number of well-established ground control techniques, including reorientation of openings relative to the prevailing orientation of the maximum horizontal compressive stress, σ_H, and stress shadowing [9]. Of course, once the excavation in the subsurface is introduced, the local stress state is perturbed on a finer scale (Fig. 1C). The perturbation of the stress field at this scale depends on the local driving stress (from the regional perturbation), the geometry of the mine opening(s), the rock mechanical properties, and the presence of structural discontinuities (joints, faults, bedding interfaces). It is this local stress perturbation which ultimately determines the stability of the mine opening. In an ideal situation, it would be beneficial for the mining engineer to estimate the state of stress on the regional scale prior to excavation, and use this information to calculate the local perturbation should an entry of a particular geometry be excavated.

3. Field area and geologic setting

The case-study area for our investigation lies in Carroll County, Ohio, in the western half of the Appalachian Plateau geologic province within the Appalachian Sedimentary Basin, although the

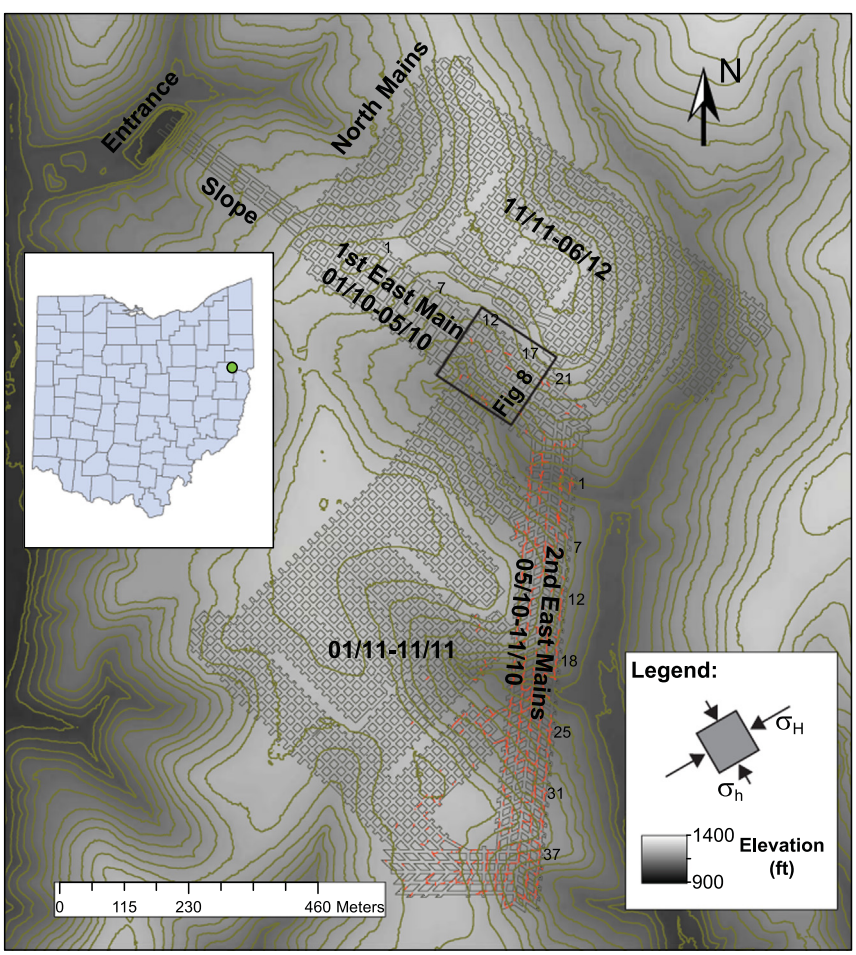

Fig. 2. Location of the study area, and overlay of topography over the mine map. Dates of completion are noted in each portion of the mine map.

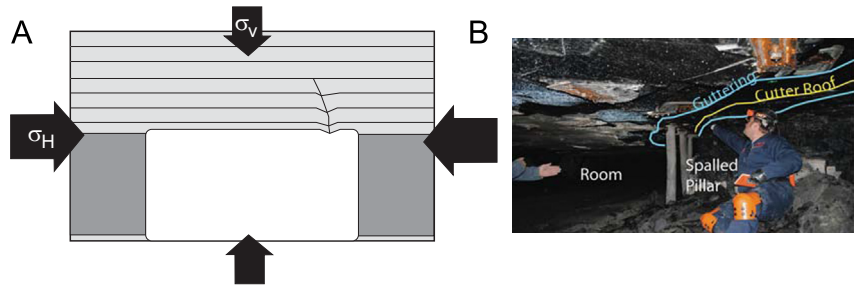

Fig. 3. Occurrence of cutter roof in the Carroll Hollow mine and model for cutter roof formation.

approach developed herein is broadly applicable to mines throughout the world. Geologically, the Appalachian Plateau is defined as the transition zone between intense deformation of the Valley and Ridge Province, manifested by twisting and faulting of the bedrock to the east, and weakly deformed rocks to the west. The Appalachian Plateau region is defined by rolling topography above broad folds in the rock layers, and blind thrust faults which cut the rocks at depth. These faults are rarely exposed at the surface and can cause local roof instabilities when cut by mine workings [32].

The Carroll Hollow Mine utilizes the room and pillar mining method and exploits the Middle Kittanning Coal (MKC) Seam (Fig. 2). The MKC in northeast Ohio is part of the Allegheny Formation and is middle Pennsylvanian (300–320 Ma.) in age. The actively-mined coal seam is found between 50 and 150 m below the present earth surface. It is overlain by thick black carbonaceous oil shale (cannel shale) grading up to a siderite ($FeCO_3$)-rich shale which is in turn overlain by a sandy shale/sandstone [33]. Each of these units represents a mechanical layer separated by structural discontinuities that often form the detachment surface for roof falls in the mine. Of particular concern is a thin shale layer of ~40 cm thickness which forms the immediate roof. The upper contact of this roof shale is formed by a ~1 cm thick clay layer, which serves as a major structural discontinuity prone to detachment from the overlying layers. Individual rooms are roughly 6 m wide and the seam thickness (room height) ranges from 0.8 to 1.1 m. The mine exhibits several roof control issues which are thought to be related in large part to elevated horizontal compressive stress beneath overlying valleys, with the most common issue being cutter roof failure (Figs. 2 and 3), a feature distinguished by a sub-vertical fracture extending from the roof-rib intersection upward into stratigraphic layers[34]. Cutter roof failure is thought to nucleate due to beam instability in thin roof layers, and subsequent fracturing allows roof members to delaminate (Fig. 3A), initially resulting in guttering (local delamination and fall of roof rocks) around the fracture, and ultimately leading to roof collapse (Fig. 3B) [6,34]. In Fig. 2, the mine entrance is in the northwest corner of the map area and the slope from the entrance is at a ~9° incline. Red lines denote areas of documented cutter roof failure. Cutter roof failure was generally focused in the eastern portion of the 1st East Mains and the entire length of the 2nd East Mains (Fig. 2). In the Carroll Hollow mine, areas prone to cutter roof failure are also prone to spalling of coal pillars (Fig. 3B).

4. Methods

4.1. Boundary element method (BEM)

The BEM is a unique numerical technique for modeling problems in solid mechanics, and has been used in mining applications for over three decades. In this study we model stress perturbations due to irregular topography (and, potentially, geologic structures) using *Poly3D*, a 3D BEM in which 3D surfaces can

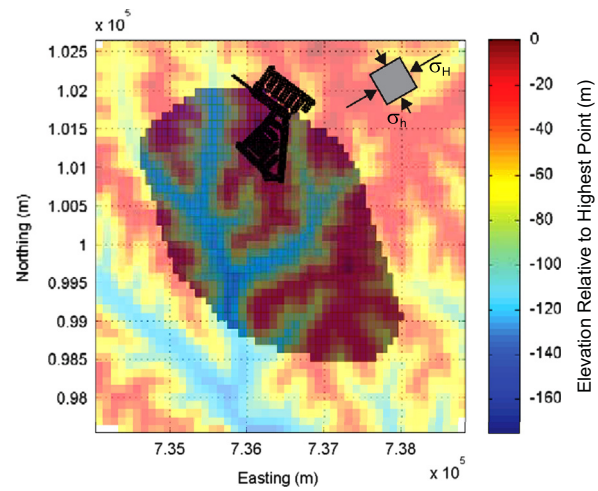

Fig. 4. Model geometry, including the topographic surface (contoured) and the coal seam/roof shale bedding discontinuity below.

be discretized into 2D polygons, allowing for accurate depictions of surfaces of any geometry (Fig. 4) [30,35,36] *Poly3D* can solve for the stress, strain, and displacement fields throughout an otherwise isotropic, homogeneous body as long as the boundary conditions (i.e., tractions or displacements) are prescribed along the model surfaces. For the case of the current application, the state of stress at any point in the subsurface is a result of the superposition of vertical gravitational stresses and the far-field tectonic stresses. Because the topographic surface is irregular, the gravitational component of stress will be non-uniform throughout the model. The stress field beneath a topographic surface can be calculated by subtracting the gravitationally induced stresses imposed by the overburden on the underlying material from the stresses in a semi-infinite body [30]. The resulting model is one in which the tractions acting normal to the topographic surface are zero, and the stresses beneath the free surface are non-uniform beneath an arbitrary topographic profile. As a BEM code, *Poly3D* only requires discretization of the discontinuities forming the model boundaries, rather than volumetric meshing of surrounding rock as required by the FEM. Consequently, this code facilitates easy manipulation of model geometry [31,35,37], and computation time for the simulations conducted in this study is less than an hour on a standard desktop PC.

4.2. Geometry and boundary conditions

For simulations of the heterogeneous stress field throughout the mine, several inputs are required, including (1) the geometry of the topographic surface which constitutes the model boundary in our simulations (Fig. 4), (2) the regional tectonic stress state (Fig. 1B), and (3) the elevation of points on the target layer throughout the area of interest: the "observation points" at which

perturbed stresses that act on the mine workings are calculated (Fig. 4). The discretized topographic surface has been created using an *XYZ* point cloud derived from freely available Light Detection and Ranging (*LiDAR*) data from the Ohio Statewide Imagery Program (⟨http://ogrip.oit.ohio.gov/ProjectsInitiatives/StatewideImagery.aspx⟩). For modeling purposes the *XYZ* point cloud is discretized into a mesh consisting of triangular elements using Delaunay triangulation tools within *Matlab*©. An example of the topographic surface derived from this dataset for the region surrounding the Carroll Hollow Mine is shown in Fig. 4. The triangular elements in the simulation mesh had a roughly uniform edge size of ~40 m, smaller than the minimum depth to the coal seam. Preliminary mesh sensitivity investigations showed that decreasing triangle size had little effect on stress calculations on the coal seam. Furthermore, the lateral extent of the topographic model surface extends far beyond the lateral tips of the model coal seam surface in order to minimize tip effects on stresses calculated on the coal seam. The coal seam elevation is derived from a combination of exploratory borehole data and in-mine surveying of the active mine workings, and the resulting 3D surface shown in Fig. 4 is constructed using the resulting point cloud in the same manner as the topographic surface, although it should be stressed that unlike the topographic surface, the coal seam surface is merely a set of observation points at which stresses and displacements are calculated, not a discontinuity required to satisfy local traction boundary conditions. The regional stress state has been devised from published data as discussed below.

The state of stress in the Appalachian Basin in eastern Ohio and Western Pennsylvania is characterized by a horizontal maximum compressive stress, σ_H, which trends roughly N60°E [38] (Fig. 4). The stress regime is stratified: at depths greater than approximately 1 km, the vertical normal stress, σ_v, exceeds the intermediate principal stress σ_h, therefore the Andersonian stress regime is one of strike slip faulting [39]. At shallower depths typical of coal mining in the region, however, $\sigma_H > \sigma_h > \sigma_v$ and the shallow crust is subject to a thrust faulting stress regime [40,41]. Near the earth's surface, the relationship between the magnitude of principal stresses and depth is difficult to predict as it can be highly variable. In a classic Andersonian thrust faulting stress regime, the minimum compressive stress direction is vertical (σ_v), the maximum compressive stress σ_H is horizontal, and the intermediate principal stress is σ_h, also horizontal. Several investigations of the *in-situ* stress state of the crust at depth have suggested that the crust is critically stressed, that is, pre-existing faults and fractures are stressed just to the point of frictional failure [14,42,43]. Following this assumption, a reasonable starting point for a stress state characterized by thrust faulting can be calculated at a particular depth by assuming that σ_v is equivalent to the overburden stress, the magnitude of σ_H and σ_h are such that an optimally oriented thrust fault would be at its critical threshold for frictional slip [42]. This requires the assumption that $\sigma_h=(\sigma_H+\sigma_v)/2$, i.e., that the intermediate principal stress is equal to the mean normal stress. Assuming that the crust is critically stressed, a common assumption based on abundant direct stress measurements in the upper crust [43], both σ_H and σ_h can be calculated assuming an approximate Byerlee friction coefficient of $\mu \approx 0.75$ [44]. In this paper this stress model is described as Model A, the "frictional constraint" model (Fig. 5), and the equations for each stress term are summarized in Table 1. One particular problem with the frictional constraint model is that all stress components decay to zero at the earth's surface; however evidence from direct shallow stress measurements in Ohio suggests this is not typically the case [45]. In order to produce a more realistic representation of stress magnitudes in the shallow crust, Mark and Gadde [46] compiled a large database of *in situ* stress measurements from mining regions around the world, and conducted a series of linear regressions to derive empirical equations for vertical gradients in each of the three principal stress components (σ_H, σ_h, and σ_v). Regressions were performed for each major coal producing region in the world for which data was available. The resulting empirical equations for the Appalachian Basin region are given in Table 1 and shown in Fig. 5 where the Mark and Gadde [46] stress model is referred to as Model B.

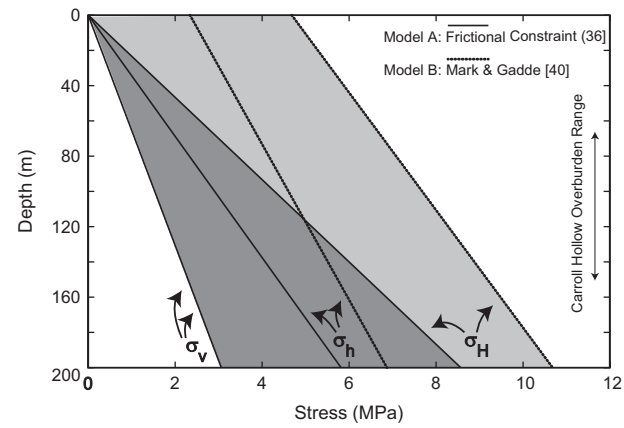

Fig. 5. Global stress state models for northeast Ohio, including the Model A, the frictionally constrained model [42] shaded in dark gray solid lines, and Model B based on Mark and Gadde [46] shown in light gray and dashed lines.

Table 1
Stress boundary conditions. Relevant terms are density (ρ) in kg/m^3, acceleration due to gravity (g) in m/s^2, elevation relative to the highest point in the model (z) in m (see Fig. 4B and Fig. 5), and a dimensionless pore-fluid factor (λ) which represents the ratio of pore-fluid to rock density.

Model	σ_H (MPa)	σ_h (MPa)	σ_v (MPa)	Reference
A	$3\rho gz(1-\lambda)\times 10^{-6}+\sigma_v$	$(\sigma_H+\sigma_v)/2$	$\rho gz(1-\lambda)\times 10^{-6}$	[36]
B	$2.6+0.03z+2.08$	$(\sigma_H+\sigma_v)/2$	$\rho gz(1-\lambda)\times 10^{-6}$	[40]

Because we take a multi-scale modeling approach in this paper, differentiating the stress terms at each stage of the modeling process can be somewhat confusing. For clarity, throughout the remainder of this paper, we will refer to the global, far-field principal stresses (Fig. 1A) as σ_H, σ_h, and σ_v. These will constitute the far-field stresses which drive deformation in simulations of topographic stress perturbations using *Poly3D*. Because the resulting perturbed stress fields along the coal seam are no longer constrained to be vertically and horizontally oriented, we adopt the terminology of σ_1, σ_2, and σ_3 for the regionally-perturbed maximum compressive, intermediate, and least compressive principal stresses calculated by our *Poly3D* model. Far-field boundary conditions are prescribed as stress gradients σ_H, σ_h, and σ_v, all of which increase linearly with depth, and are defined for each model in Table 1. For these calculations we assume average density $\rho=2500$ kg/m^3 for the packages of sedimentary rocks overlying the mine (limestone, sandstone, shale), pore fluid factor $\lambda=0.4$, and acceleration due to gravity $g=10$ m/s^2. Like density, elastic rock properties are chosen to represent average expected properties of the sedimentary cover, Young's modulus $E=30$ GPa and Poisson's ratio $\nu=0.2$.

5. Results

Aspects of the computed stress fields along the coal seam based on Model B are plotted in Figs. 6 and 7. Calculated stress fields based on Model A are similar to those based on Model B and, because we prefer the better-constrained global stress state of

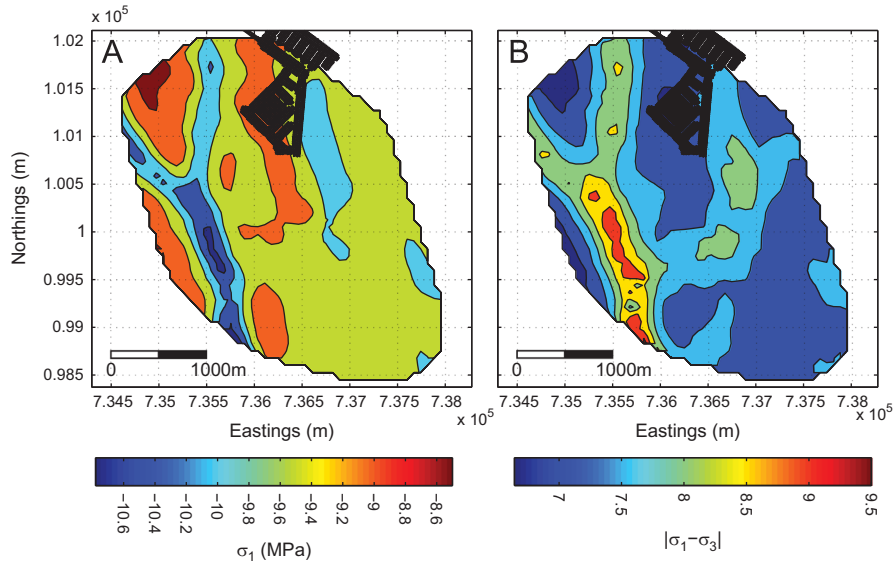

Fig. 6. Magnitudes of regional principal stresses at the coal seam elevation perturbed by overlying topography including (A) Magnitudes of greatest principal compressive stress σ_1 and (B) differential stress $|\sigma_1-\sigma_3|$.

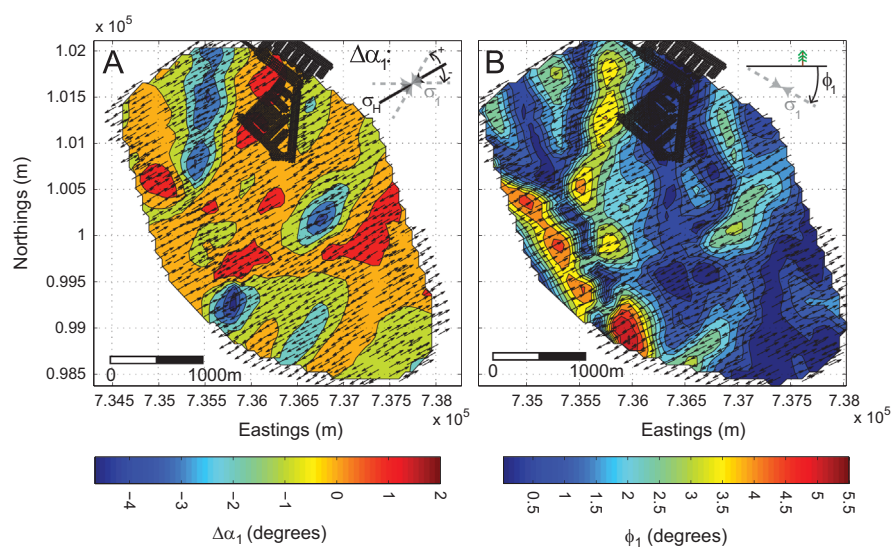

Fig. 7. Angular variations of topographically perturbed principal stresses. (A) Deviation ($\Delta\alpha_1$) of the azimuth (horizontal angle) of σ_1 from that of the far-field maximum horizontal compressive stress σ_H. (B) Inclination (vertical angle, ϕ_1) of σ_1. In both plots, arrows point in the direction that stress trajectories are inclined below horizontal.

Model B, we omit the results of Model A for brevity. It is observed from Figs. 6 and 7 that the stress magnitudes are highly heterogeneous, with the maximum perturbed compressive stress σ_1 varying locally by as much as 2.7 MPa. As expected σ_1 generally increases beneath valleys, and decreases beneath ridges in all models. Peak differential stress approaches the magnitude of σ_1, indicating that σ_3 in those locations is close to zero. The 2nd East Mains corridor (Fig. 2), the site with most intense cutter roof failure, is coincident with a region of elevated σ_1 relative to the average value (Fig. 6A). The largest magnitude of σ_1 occurs along a large north–south trending valley on the western side of the coal seam along the 2nd East Mains (Figs. 2 and 6A). Variations in stress magnitude are less extreme in the region of the existing mine, however areas of mapped cutter roof occurrence (Figs. 2 and 3) do correspond to areas of more compressive-than-average magnitudes of σ_1.

Principal stress directions deviate from the remote stress orientation in both Models A and B, in terms of azimuth and inclination (principal direction). Deviations ($\Delta\alpha_1$) of the azimuth of σ_1 from σ_H can be as great as 6.9° in Model A and 5.5° in Model B, whereas inclination (ϕ_1) of σ_1 could be as great as 4.1° in Model A and 5.7° in Model B (Table 2). Unlike the variation of stress magnitude, where larger magnitudes of σ_1 typically occur beneath valleys, variation in azimuth and inclination of σ_1 is less intuitive. Comparing Fig. 7A with Fig. 4, variations in σ_1 azimuth $\Delta\alpha_1$ tend to be negative in sign and larger magnitude beneath valleys, as compared to $\Delta\alpha_1$ beneath ridges; but the degree of azimuth deviation varies significantly depending on the valley trend and nearby topography. Variations in σ_1 inclination ϕ_1 are perhaps more intuitive, in that σ_H generally plunges toward the valley floor, away from ridges; however like patterns of $\Delta\alpha_1$, the magnitude of ψ_1 depends largely on the trend of the valleys relative to the azimuth of σ_H (ϕ_1 is the greatest when the valley trend is roughly perpendicular to the trajectory σ_H). The range in stress azimuth is not likely be significant in terms of mine planning, as a variation of $\Delta\alpha_1$ ($<6°$) is probably within the range

Table 2
Representative perturbed stress results. For fully-perturbed stress fields, see Figs. 6 and 7.

	Max (σ_1) (MPa)	Min (σ_1) (MPa)	Ave (σ_1) (MPa)	Max (σ_d) (MPa)	Ave (σ_d) (MPa)	Max (ϕ_1)	Ave (ϕ_1)	Max ($\Delta\psi_1$)
Model A	10.8	8.6	9.6	10.5	8	4.1°	1.1°	6.9°
Model B	11	8.3	9.3	10.5	7.6	5.7°	1.7°	5.5°

of error encountered in practice when cutting pillars in any particular orientation. As shown in the next section, however, the simulated variance in ϕ_1 is quite significant in predicting patterns of stress-related roof failure.

6. Discussion

It has been long understood that "valley stresses", or amplified magnitudes of the horizontal compressive stress relative to average global values, increase the risk of ground control problems in shallow underground mines. However, the exact manifestation of these "valley stress" perturbations has not received a significant amount of attention in the literature, particularly not for realistic 3D geometries. As shown in the previous section, for the Carroll Hollow mine, the magnitude of the greatest compressive stress σ_1 may vary by as much as 30% of its peak value (Fig. 6), the azimuth may vary as much as 6°, and the inclination may vary by as much as 5°. In other regions in the Appalachian Basin with greater topographic relief at the earth's surface (western Pennsylvania, West Virginia, Kentucky), these deviations from the regional principal stress magnitude and direction are expected to be more significant, particularly for mines with average overburden thickness comparable to the Carroll Hollow mine (~50–150 m).

In an attempt to both verify that the computed stress fields are realistic, and to demonstrate the utility of the approach of computing topographic stress perturbations, we have conducted simulations of the effect of the topographically perturbed stresses on local stress distribution around openings at the scale of individual rooms in the mine (Fig. 1C). In order to verify the calculated stresses, we surveyed the local mine geometry, including roof failures, in a section of the mine where cutter roof and related guttering have been observed (Fig. 8). Note that the location of Fig. 8 is indicated by a box along the 1st East Mains in Fig. 2. As part of the site selection, we constructed 2D vertical NE–SW slices of the mine geometry through rooms/pillars between entries 14 and 15 as well as 15 and 16 (Fig. 8). These sections were selected because cutter roof and guttering were observed along them, their cross-section makes a reasonably small angle with the orientation of σ_H in the region, and this section of the active mine was accessible during surveying. Furthermore, the pillars are cut at approximately 90° angles, allowing for plane strain modeling of stresses in a 2D cross section as a rough approximation. The geometry of the mine openings along each slice were produced by use of a radial laser surveying device designed for cave surveying [47]. Using this device, we reproduced the true aspect ratio of each room in the cross-section [48]. For modeling purposes, we ignored the presence of gutters, and we assumed that the original, undeformed excavation geometry was that of a rectangle with smooth corners. Resulting aspect ratios in these surveys were on the order of 3.8–7.7 (length to height) as summarized in Table 3 and shown graphically in Fig. 9. During surveys, we noted the presence of cutter roof and the depth and width of gutters which formed around the cutter roof fractures.

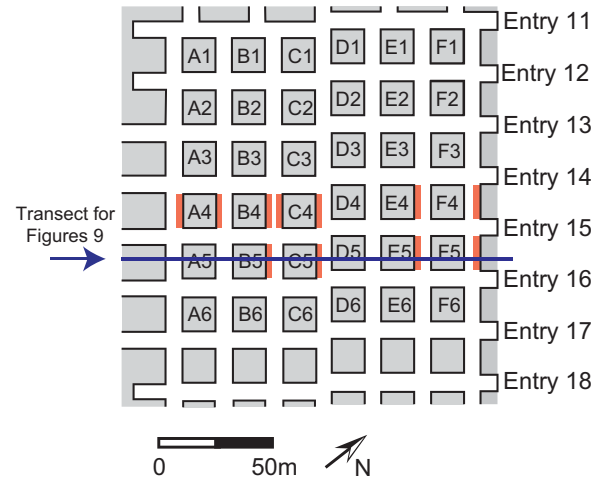

Fig. 8. Region of in-mine vertical cross-section to create the 2D local geometry of the mine openings. Location of this figure shown in Fig. 2.

Table 3
Measured aspect ratios (width to height) of openings surveyed in Carroll Hollow Mine, OH.

Entry	Height (m)	Width (m)	Aspect ratio
Wall-A4	1.32	5.02	3.80
Wall-A5	1.15	5.53	4.81
A4-B4	1.24	5.32	4.29
A5-B5	1.40	6.20	4.44
B4-C4	1.09	6.99	6.41
B5-C5	1.31	5.61	4.28
C4-D4	1.37	7.41	5.41
C5-D5	1.20	6.80	5.66
D4-E4	1.33	6.17	4.64
D5-E5	1.23	6.61	5.37
E4-F4	1.09	5.45	5.00
E5-F5	1.34	5.60	4.18
F4-Wall	1.02	4.66	4.57
F5-Wall	0.81	6.25	7.71
		Minimum ratio	3.80
		Mean ratio	5.04
		Maximum ratio	7.71

As shown in Table 4, the gutters were typically on the order of 10–30 cm deep, corresponding to the approximate thickness of the immediate shale roof thickness, and the width of the gutters scales with the gutter depth. The depth of gutters supports the interpretation that once cutter roof fractures penetrate the roof strata, guttering is a product of cantilevering of the roof layers to a stratigraphically controlled detachment. Note that the location of the gutters listed in Table 4 are shown schematically in Fig. 8. Gutters were noted on both the left (southwest) and right (northeast) corners of openings in both surveys; however 2/3 of the gutters were present on the left (southwest) side of each opening (Table 4).

Using the opening geometries constructed using the radial laser surveying technique discussed above as model boundaries, we used simple 2D, plane strain BEM simulations to calculate the stress fields associated with the introduction of the mine openings along the survey lines. In these simulations, the local mine geometry forms the model boundaries discretized into fictitious stress elements embedded in an infinite elastic medium [49]. The model boundaries are assumed to be traction-free, and the rocks are loaded by a far-field stress, corresponding to the topographically-perturbed stresses acting on the coal seam in the vicinity of the survey lines by the *Poly3D* simulations. The closest observation point on the coal seam had a calculated value of $\sigma_1 = -9.4$ MPa and

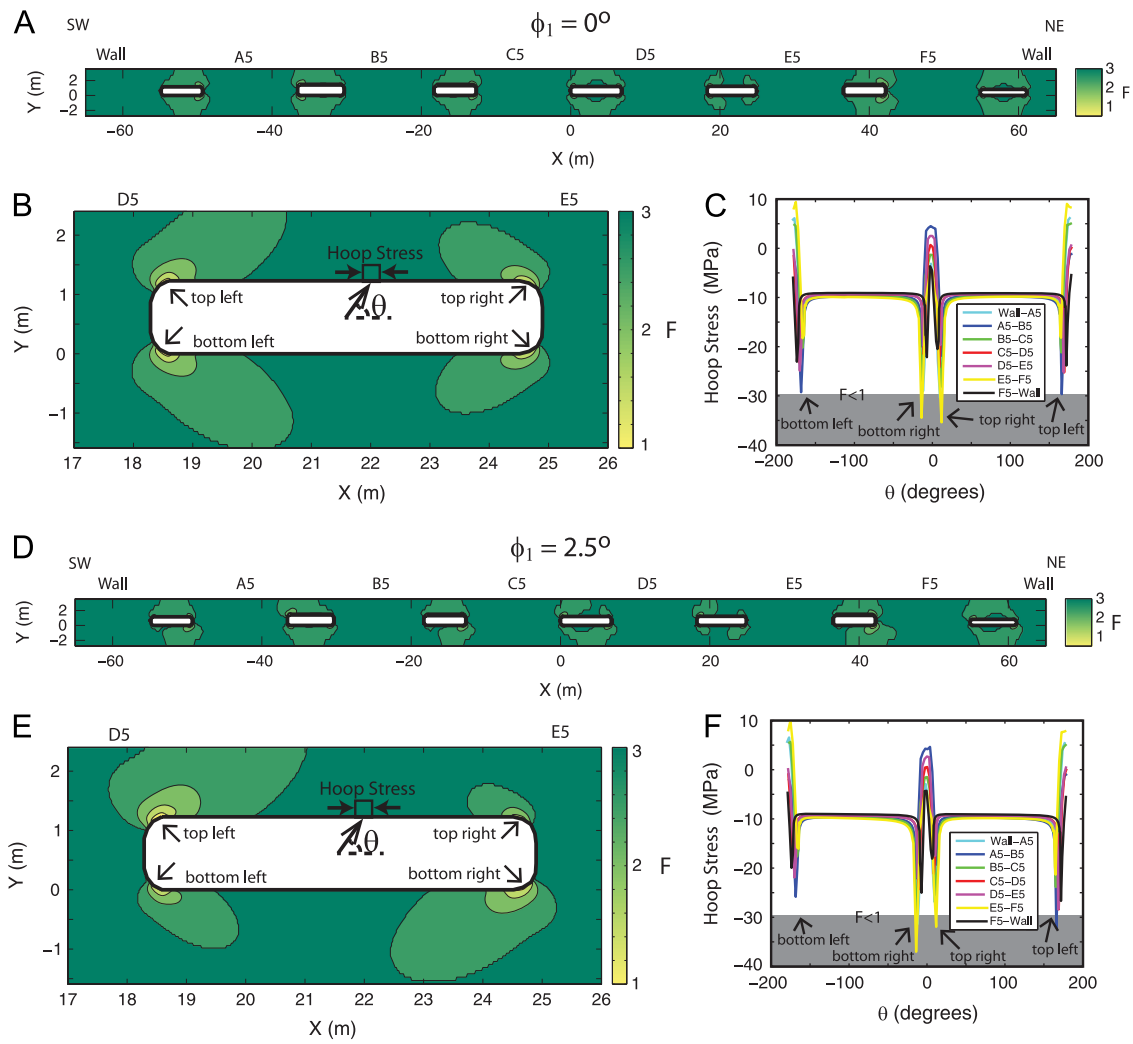

Fig. 9. Local perturbed stresses around openings along transect defined in Fig. 8 due to regionally-perturbed principal stresses. Including cases in which ((A)–(C)) $\phi=0$ (σ_1 is horizontal and σ_3 is vertical) and ((D)–(F)) $\phi=2.5^\circ$.

Table 4
Dimensions of gutters present in surveyed section of Carroll Hollow Mine.

Entry	Left pillar	Right pillar	Left gutter		Right gutter	
Name	Name	Name	Width (m)	Depth (m)	Width (m)	Depth (m)
Wall-A4	Wall	A4	N/A	N/A	0.76	0.10
Wall-A5	Wall	A5	N/A	N/A	N/A	N/A
A4-B4	A4	B4	1.05	0.09	N/A	N/A
A5-B5	A5	B5	N/A	N/A	N/A	N/A
B4-C4	B4	C4	1.19	0.20	0.81	0.03
B5-C5	B5	C5	1.60	0.28	N/A	N/A
C4-D4	C4	D4	1.98	0.15	N/A	N/A
C5-D5	C5	D5	1.06	0.08	N/A	N/A
D4-E4	D4	E4	N/A	N/A	N/A	N/A
D5-E5	D5	E5	N/A	N/A	N/A	N/A
E4-F4	E4	F4	1.09	0.33	N/A	N/A
E5-F5	E5	F5	1.37	0.23	N/A	N/A
F4-Wall	F4	Wall	1.16	0.15	1.03	0.16
F5-Wall	F5	Wall	N/A	N/A	0.89	0.15

$\sigma_3=-1.7$ MPa, with σ_1 inclined at an angle $\phi_1 \approx 2^\circ$ toward the southwest as defined in the inset in Fig. 7B. Rocks are modeled as homogeneous, linear elastic materials with Young's modulus of $E=16$ GPa, Poisson's ratio $\nu=0.29$, and uniaxial compressive strength UCS=30 MPa as determined using standard uniaxial compression tests on cylindrical specimens to failure.

It should be noted that the simulations at the local scale are intentionally simple. Our goal is to isolate the effect of topographically perturbed stresses on the local stress field around openings. We make no attempt to simulate time- or path-dependent processes such as fracture growth, fluid flow, or frictional sliding on pre-existing discontinuities. As a result of the model simplicity, we do not expect these simulations to produce precise depictions of the stresses acting in the pillars just after mining. We do, however, expect the results to give a good approximation of the typical stress magnitudes surrounding openings perturbed by the topography, and we also expect to gain some insight into the general patterns of stress perturbations in the mine.

We investigate the local stress field around mine excavations for two cases which results from the topographic perturbation. In both cases, $\sigma_1=-9.4$ and and $\sigma_3=-1.7$, values calculated in the vicinity with *Poly3D* in Figs. 6 and 7. In the first case (Fig. 9A–C), we consider σ_1 and σ_3 to be horizontal and vertical ($\phi_1=0^\circ$), respectively. In the second case (Fig. 9D–F), we consider the inclinations of these stresses ($\phi_1=2.5^\circ$) modeled using *Poly3D*. Contours of the local stress fields produced using the 2D BEM models are shown in Fig. 9A and D, calculated as a factor of safety *F*, which, following Esterhuizen et al. [44], is expressed as the ratio of the UCS to the calculated σ_1 in the model. Areas in which $F<1$

are considered to be prone to compressive/shear failure. Fig. 9B and E show a detailed view of *F* around the fifth hole, while Fig. 9C and F show the hoop stress (in-plane normal stress) as it varies with angle around the hole. In Fig. 9A, we observe some general trends which contrast from those summarized by Hill [28] under purely gravitational loading. Specifically, under pure gravitational loading, larger aspect ratios result in larger compressive stress magnitudes at the corners of rectangular excavations. When the tectonic stress component is larger than the gravitational component as is the case for the current study and mines throughout the Appalachian basin, smaller aspect ratios result in larger compressive stresses at the corners. In the case of $\phi_1=0^\circ$, compressive hoop stress magnitudes at corners of excavations are magnified by as much as a factor of 4 compared to the far-field maximum compressive stress σ_1, and the magnitude of hoop stress exceeds the UCS of the roof shale in several of the upper corners (Fig. 9B and C). Note that along floors and roof away from the corners, the hoop stress is compressive roughly equal σ_1 (Fig. 9B) because roof and floors are modeled as straight horizontal surfaces. Corners in which the magnitude of modeled hoop stress exceeds the UCS do not, in general, correspond to the locations of mapped gutters (Table 3). In the current case, hoop stress magnitudes in corners are controlled by opening aspect ratio as well as mechanical interaction between neighboring openings. On pillars, the hoop stress is tensile, reaching a magnitude of 5 MPa in the most extreme case (left side of pillar B5, Fig. 9C). This result is consistent with the common observation of pillar spalling (Fig. 3C). For the case of $\phi_1=2.5^\circ$, the distribution of hoop stress becomes asymmetric, with greater compressive values in the upper left and lower right corners as compared to upper right and lower left corners, respectively. This distribution is consistent with the general observation that 2/3 of the observed gutters associated with cutter roof failure occurred in the upper left-hand corners.

As mentioned previously, these models are highly idealized, but the efficacy of the general multi-scale modeling approach is demonstrated in several respects. First, based on the consistency between simulation and field observation of (A) areas of elevated compressive stresses in the 3D topographically-perturbed stress models and areas of mapped cutter roof failure and (B) observed asymmetry of local compressive stress concentrations and cutter roof/gutter distribution within 2D transects across the mine, the approach appears to be successful in capturing the general trends of stress perturbation throughout the mine. Second, because only the model boundaries need to be discretized, this approach is extremely efficient. Furthermore, abundant digital topography data are available for active mining regions throughout the United States. Given information about the local stress field, digital elevation data which can be converted into a 3D triangular mesh, and the geometry and elevation of the target layer, a mechanical model predicting the perturbed stress state such as that pictured in Figs. 6 and 7 can be produced in as little as one day worth of work by a well-trained scientist or engineer armed with the appropriate software. The resulting model can help mine engineers in designing mine plans which incorporate appropriate measures to mitigate ground control hazards, or to avoid hazardous areas.

There are a number of limitations to the current study approach, and these should be the focus of future work. First, 2D plane-strain simulations clearly cannot account for the stress perturbation throughout room/pillar mines [50]. Creating such 3D model geometries can be extremely cumbersome. Our 2D approach was aimed at getting a first-approximation of the stress perturbation around the local-scale excavation geometry in order to evaluate the performance of the larger-scale 3D topographic models. However, in practice it would be desirable to be able to quickly evaluate stress distributions with different 3D mine models. Furthermore, we made no attempt to model pre-existing anisotropy or material heterogeneities inherently associated with sedimentary rocks. Heterogeneities and mechanical discontinuities in the form of channel deposits, joints, and faults can cause local stress perturbations or weaken rocks significantly. Without knowing the distribution of such heterogeneities *a priori*, it is difficult to incorporate these into models; however sedimentary rocks can typically be represented satisfactorily as transversely anisotropic materials. Finally, the use of the UCS as a failure criterion describing the onset of cutter roof failure is an inherent oversimplification, particularly in anisotropic rocks. Cutter roof failure is a complex process which deserves extensive study in its own right, and a satisfactory failure criterion has not been adequately described in the literature. Addressing these limitations is the focus of our ongoing work. These include developing a new BEM model to account for rock anisotropy and layered joints surrounding excavations with realistic 3D geometries.

7. Conclusion

We calculated the topographically-perturbed stress field by taking into account both gravitational and tectonic stresses as well as complicated 3D topography, in the region of the Carroll Hollow coal mine in Carroll County, Ohio. In the region of the Carroll Hollow mine, computed maximum compressive stress can vary as much as 30%, and the maximum compressive stress direction may be inclined by more than 5°. Models of the local-mine-scale stress perturbations show that increased regional compressive stresses in some regions of the mine are large enough to induce compressive roof failure. Furthermore, the calculated stress inclinations produces asymmetries in the maximum compressive stress field which qualitatively matches the observed distribution of gutters associated with cutter roof failure in the mine. Calculation of the stress magnitudes throughout the intended mining region allows us to identify areas of high potential hazard as well as predicts asymmetry in the distribution of stress-related roof hazards. This study demonstrates the efficacy of such a multi-scale modeling approach to predicting ground control problems; however some limitations of the current approach warrant further work. Specifically, a 3D modeling tool which allows for simultaneous simulation of the topographic surface and planned mine geometries in anisotropic rock would greatly increase our ability to predict ground control hazards in the planning stages of shallow underground mines.

Acknowledgements

This work has been conducted with support from the National Institute for Occupational Health and Safety award # 5R03OH010112-02 to Griffith and Pan. We acknowledge the East Fairfield Coal Company and E. Bleakney for access to the mine, data, and physical resources necessary to complete this work. G.S. Esterhuizen provided suggestions on an earlier draft of the manuscript, and reviews were provided by L. Alejandro, and two anonymous reviewers. Z. Hakke provided field assistance, and T. Quick is thanked for technical assistance in the lab at the University of Akron.

References

[1] 〈http://www.msha.gov/stats/charts/coal2011yearend.asp〉, 2013.
[2] Moebs NN, Stateham RM. Geologic factors in coal mine roof stability-a progress report. USBM IC 8976, 1984, 27 pp.
[3] Molinda GM, Heasley KA, Oyler, DC, Jones JR. Effects of horizontal stress related to stream valleys on the stability of coal mine openings. USBM RI 9413, 1992, 92–97.

[4] Enever JR, McKay J. Stress measurements at Nattai North Colliery and their interpretation in terms of sedimentological and topographic features. CSIRO Rep 29, 1980, 27.
[5] Bauer ER. The effects of valleys on the strength of rock materials at depth. In: Proceedings of the 28th U.S. symposium on Rock Mechanics, Tucson, 1987, p. 345–389.
[6] Molinda GM, Mark C. Ground failures in coal mines with weak roof. Electron J Geotech Eng 2010;15:547–88.
[7] Molinda, GM. Geologic hazards and roof stability in coal mines, NIOSH information circular IC9466, 2003, 33.
[8] Bucky PB. Use of models for the study of mining problems. Am Inst Min Metall Eng Tech Pub 1931;425.
[9] Bucky PB, Taborelli RV. Effects of immediate roof thickness in longwall mining as determined by barodynamic experiments. Trans Inst Min Metall 1938: 130–314.
[10] Evans WH. The strength of undermined strata. Trans Inst Min Metall 1941;50: 475–500.
[11] Sofianos AI. Analysis and design of an underground hard rock Voussoir Beam roof. Int J Rock Mech Min Sci 1996;33(2):153–66.
[12] Hatzor YH, Benary R. The stability of a laminated Voussoir Beam: back analysis of a historic roof collapse using DDA. Int J Rock Mech Min Sci 1998;35(2): 165–81.
[13] Tsesarsky M. Deformation mechanisms and stability analysis of undermined sedimentary rocks in the shallow subsurface. Eng Geol 2012;133–134:16–29.
[14] Zoback ML. First- and second-order patterns of stress in the lithosphere: the World Stress Map Project. J Geophys Res 1992;107(B8):11703–28.
[15] Mucho TP, Mark C. Determining horizontal stress direction using the stress mapping technique. In: Proceedings of the 13th conference on ground control in mining, Morgantown, 1994, p. 277–289.
[16] Dolinar D. Variation of horizontal stresses and strains in mines in bedded deposits in the eastern and Midwestern United States. In: Proceedings of the 22nd international conference on ground control in mining, Morgantown, 2003, p. 178–185.
[17] Iannacchione AT, Dolinar DR, Prosser LJ, Marshall TE, Oyler DC, Compton CS. Controlling roof beam failures from high horizontal stresses in underground stone mines. In: Proceedings of the 17th international conference on ground control in mining, Morgantown, 1998, p. 102–112.
[18] Mushkelishvilli NI. Some basic problems of the mathematical theory of elasticity. Leyden: Noordhoff; 1953; 732.
[19] Savage WZ, Swolfs HS, Powers PS. Gravitational stresses in long symmetric ridges and valleys. Int J Rock Mech Min Sci 1985;22:291–302.
[20] Savage WZ, Swolfs HS. Tectonic and gravitational stresses in long symmetric ridges and valleys. J Geophys Res 1986;91:3677–85.
[21] Savage WZ. Gravity-induced stresses in finite slopes. Int J Rock Mech Min Sci 1994;31:471–83.
[22] Pan E, Amadei B. Gravitational stresses in long asymmetric ridges and valleys in anisotropic rock. Int J Rock Mech Min Sci 1993;30:1005–8.
[23] Pan E, Amadei B. Stress concentration at irregular surfaces of anisotropic half-space. Acta Mech 1995;113:119–35.
[24] Pan E, Amadei B, Savage WZ. Gravitational stresses in long symmetric ridges and valleys in anisotropic rock. Int J Rock Mech Min Sci 1994;31:293–312.
[25] Pan E, Amadei B, Savage WZ. Gravitational and tectonic stresses in anisotropic rock with irregular topography. Int J Rock Mech Min Sci 1995;32:201–14.
[26] Amadei B, Pan E. Role of topography and anisotropy when selecting unlined pressure tunnel alignment. J Geotech Eng 1995;121:879–85.
[27] Su WH, Peng SS. Cutter roof and its causes. Min Sci Tech 1987;4:113.
[28] Molinda GM, Heasley KA, Oyler DC, Jones JR. Effects of horizontal stress related to stream valleys on the stability of coal mine openings. U.S. Bureau of Mines RI 9413, 1992, 26.
[29] Martel SJ. Modeling elastic stresses in long ridges with the displacement discontinuity method. Pure Appl Geophys 2000;157:1039–57.
[30] Martel SJ, Muller JR. A two-dimensional boundary element method for calculating elastic gravitational stresses in slopes. Pure Appl Geophys 2000;157:989–1007.
[31] Thomas AL. Poly3D: a three-dimensional, polygonal element, Displacement Discontinuity Boundary Element Computer Program with applications to fractures, faults, and cavities in the Earth's crust. Master's thesis. Stanford University, Stanford, California, 1993, 52 pp.
[32] Phillipson SE. Effects of late Paleozoic foreland deformation on underground coal mine instability, Illinois and Appalachian Basins. Int J Coal Geol 2005;64:2–19.
[33] Coogan AH. Ohio's surface rocks and sediments. In: Feldmann RM and Hackathorn M, editors, Fossils of Ohio: Ohio Division of Geological Survey, 2007. p. 1–21.
[34] Hill JL. Cutter roof failure: an overview of the causes and methods for control. USBM IC 9094, 1986. 27.
[35] Griffith WA, Cooke ML. Mechanical validation of the three-dimensional intersection geometry between the Puente Hills Blind-Thrust System and the Whittier Fault, Los Angeles, California. Bull Seismol Soc Am 2004;94: J-M.Daniel. Three-dimensional geomechanical modeling for constraint of subseismic fault simulationAm Assoc Petrol Geol Bull 2006;94:1337–58.
[37] Crider JG, Pollard DD. Fault linkage: 3D mechanical interaction between overlapping normal faults. J Geophys Res 1998;103:24,373–91.
[38] Plumb RA, Cox JW. Stress directions in eastern North America determined to 4.5 km from borehole elongation measurements. J Geophys Res 1987;92 (B6):4805–16.
[39] Anderson EM. The dynamics of faulting. Revised ed.. London: Edinburgh Publishing; 1951.
[40] Hancock PL, Engelder T. Neotectonic joints. Geol Soc Am Bull 1989;101: 1197–208.
[41] Evans MA. Joints and decollment zones in Middle Devonian shales: evidence for multiple deformation events in the central Appalachian Plateau. Geol Soc Am Bull 1994;106:447–60.
[42] Sibson RH. Frictional constraints on thrust, wrench and normal faults. Nature 1974;249:542.
[43] Townend J, Zoback MD. How faulting keeps the crust strong. Geology 2000;28 (5):399–402.
[44] Byerlee JD. Friction of rocks. Pure Appl Geophys 1978;116(4–5):615–26.
[45] Haimson BC. Deep stress measurements in three Ohio quarries and their comparison to near surface tests. In: 23rd Symposium on Rock Mechanics, Berkeley, 1982. p. 190–2002.
[46] Mark C, Gadde M. Global trends in coal mine horizontal stress measurements. In: 27th International conference on ground control in mining, Morgantown, 2008. p. 1–13.
[47] Sasowsky I, Bishop M. Empirical study of conduit radial cross section determination and representation methods on cavernous limestone porosity characterization. J Cave Karst Stud 2006;68:130–6.
[48] Becker JB. A combined field, laboratory, and numerical study of cutter roof failure in Carroll Hollow Mine. MS thesis. The University of Akron, Akron, Ohio, 2013, 144 pp.
[49] Crouch SL, Starfield AM. Boundary element methods in solid mechanics. London: Allen and Unwin; 1983; 322.
[50] Esterhuizen GS, Dolinar DR, Iannacchione AT. Field observations and numerical studies of horizontal stress effects on roof stability in US limestone mines. In: Proceedings of the sixth international symposium on ground support in mining and civil engineering construction, Cape Town, 2008. p. 103–118.